IEICE Proceeding Series

Intrinsic Localized Mode in an Electric Lattice Containing MOS-Capacitors

W. Shi, S. Shige, H. Hasebe, M. Sato, A. J. Sievers

Vol. 2 pp. 330-333
Publication Date: 2014/03/18
Online ISSN: 2188-5079

Intrinsic Localized Mode in an Electric Lattice Containing MOS-Capacitors

W. Shi†, S. Shige†, H. Hasebe†, M. Sato†, and A. J. Sievers‡

†Graduate School of Natural Science and Technology, Kanazawa University
Ishikawa 920-1192, Japan
‡Laboratory of Atomic and Solid State Physics, Cornell University
Ithaca, New York 14853-2501, USA
Email: msato@kenroku.kanazawa-u.ac.jp

Abstract– We have succeeded in generating intrinsic localized modes (ILMs) in an electric lattice, containing nonlinear MOS-capacitors. The MOS capacitor has a larger capacitance at a larger voltage, so that the resonance frequency of the capacitor-inductor combination decreases with increasing amplitude. The ILM is phase locked to an AC driver in the auto-resonant state. Because of the soft nonlinearity of the MOS capacitor the ILM frequency is below the bottom of the dispersion curve of the linear spectrum.

1. Introduction

Intrinsic localized modes (ILMs) or discrete breathers have been reported in diverse nonlinear lattice systems. [1] The experimental demonstration of ILMs have been achieved for a variety of systems, including Josephson junction arrays [2,3], antiferromagnetic lattices [4], optical guided waves [5], micromechanical arrays [6], and three-dimensional crystals [7-9]. In a driven 1-D micromechanical array, a stationary ILM whose frequency is locked to the driver is a steady state feature [10] since the ILM amplitude is controlled by the driver frequency. This autoresonant (AR) state [11-14] is terminated at two bifurcation transitions. The bifurcation dynamics of such an AR ILM state has been analyzed in detail by using linear response spectroscopy. [11]

Another important way to study ILMs is with a nonlinear transmission line (NLTL). Researchers have been investigating such ILMs by using a diode as the nonlinear electrical element in the NLTL. The capacitance of the diode, which varies with applied voltage, can be separated into junction capacitance and diffusion capacitance. The junction capacitance dominates for reverse-biased diodes, which has been used for some research on both solitons [15-17] and ILMs [18-20], while diffusion capacitance dominates the forward-biased diode [21] producing a soft nonlinearity for the study of ILMs. [22]

In this paper we have investigated the possibility of using a MOS-capacitor as a nonlinear element. We have also made linear response measurement in such an electronic lattice. With the applied DC voltage sweeping slowly from a minus value to a suitable plus voltage, the state of the MOS-capacitor changes as follows: accumulation, depletion, and inversion. From depletion to inversion, the capacitance increases suddenly and almost immediately achieves a saturation state.[23] This variation provides sufficient nonlinearity for the production of ILMs.

With these experiments we show that a stationary ILM can be generated and maintained by the driver in the steady state. We also identify the bifurcation dynamics by measuring the linear response spectrum. We show that the behavior of the natural frequency (NF)[24] of the ILM plays an important role at both bifurcation points. Particularly interesting is the lowest frequency transition point, which occurs when the NF intersects the ILM driver frequency.

2. Experiments

Figure 1(a) shows capacitance as a function of the applied DC voltage of the MOS capacitor C_1. To make the capacitance symmetric, C_1 is formed from two anti-paralleled MOS-FETs as shown in the inset. The result is a larger capacitance at both sides of DC bias voltage and a small capacitance at the middle of the curve. The sudden change of the capacitance produces the large nonlinearity for ILM generation. The nonlinearity of C_1 can be approximated by the form of

$$C_1(V) = k_0 + k_1 \exp[-(V / k_2)] \qquad (1)$$

where k_0 =1.636nF, k_1 =-0.298nF and k_2 =2.53V. The calculated results from Eq. (1) are shown by the dashed curve in Fig. 1(a).

Our nonlinear electrical lattice is composed of 16 sections, each of which consists of a nonlinear resonator made by the nonlinear capacitor C_1, a coil (L_1=313μH) and a linear coupling element formed by a capacitor (C_2=421pF) and inductor (L_2=626μH), as shown in the inset in Fig. 1(b). The linear dispersion relation for such a nonlinear electrical lattice, shown in Fig. 1(b), is calculated from Eq. (2), which has the form

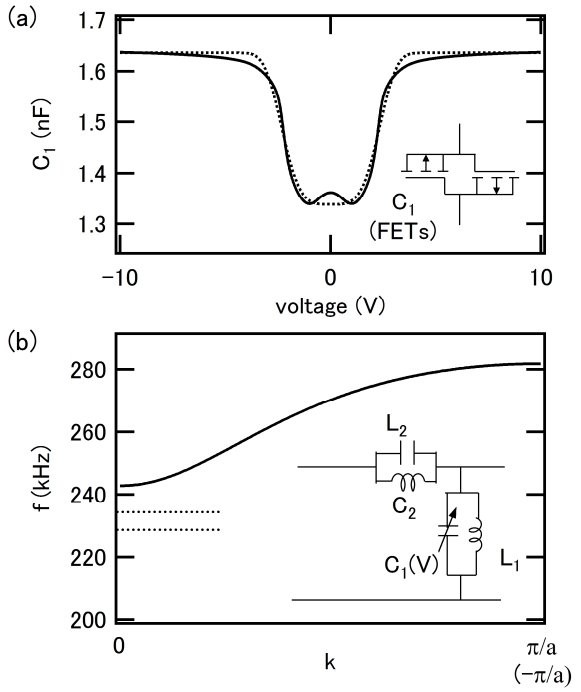

Fig. 1: (a) DC voltage dependence of the capacitance of C_1. The solid curve is for the nonlinear capacitor C_1 composed of two anti-parallel connected FETs as shown in the inset. The dashed curve is obtained using Eq. (1). (b) Linear dispersion relation curve for this 16 element electrical lattice. A typical cell of the circuit is shown in the inset, containing a coupling element, C_2 and L_2, and a resonating element, C_1 and L_1. The two dashed lines indicate the frequency range of the ILM.

$$\omega^2 = \frac{\frac{2}{L_2}(1-\cos ka)+\frac{1}{L_1}}{2C_2(1-\cos ka)+C_d+k_0+k_1} \qquad (2)$$

where C_d=34.3pF insures a weak coupling between the oscillator F and the circuit. (Neither of these elements is shown in the Fig. 1(b) insert.) The cw driver F (7V) compensates for damping to maintain the ILM in the large amplitude state. Since C_1 has a soft nonlinearity, an ILM can be generated below the bottom of the band. The ILM region is indicated by two dashed lines.

The experimental procedure is as follows: first, the cw driver excites the nonlinear electrical lattice; then, the voltage of the MOS-FETs at each site is measured by an oscilloscope through a 16 channel analog multiplexer. For clarity only the absolute value of the AC voltage amplitude at each site is monitored. The localized voltage response as a function of frequency in the nonlinear lattice is shown in Fig. 2. Panel (a) is obtained by increasing or decreasing the driver frequency from an initial frequency (232 kHz), where an ILM is generated. The frequency region of a stable ILM is from 228.3 kHz to 234.7 kHz. Figure 2(b) shows an up scan case from a frequency below the stable ILM region. No ILM appears until a frequency of 231.6 kHz and then it disappears at 234.7 kHz. The maximum amplitude at each driver frequency of Fig. 2(a) and (b) is summarized in Fig. 2(c). The two bifurcation points, identified by the edges in the solid curve, define the stable ILM region.

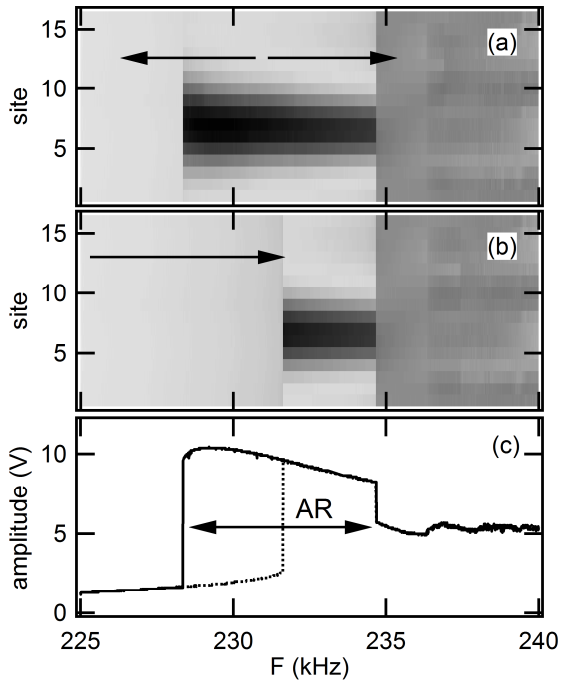

Fig. 2(a): The voltage amplitude at the different lattice points as a function of the driver frequency. Darker represents a larger voltage. The driver frequency is up-scanned or down scanned from an ILM state at 232 kHz as denoted by two arrows. The frequency range of the stable AR state is from 228.3 kHz to 234.7 kHz. (b) Like (a) but for the case of up scan from a lower frequency (225 kHz) outside the stable ILM region. (c) The maximum amplitude of the ILM as a function of the driver frequency. The solid curve is obtained from (a) and the dashed curve is measured from (b). Two bifurcation points occur for each curve.

An additional weak probe oscillator at frequency f_p is applied for the linear response measurement. Its amplitude is less than 1/1000 of the driver so that it doesn't destroy the ILM state. In order to observe the first linear local mode associated with the ILM, the probe perturbation is only applied at one lattice site contiguous with the ILM and the output signal of the other site next to the ILM is measured with a lock-in amplifier. The driver frequency is tuned by 0.2 kHz step inside the stable ILM region and the probe frequency is scanned slowly over the appropriate frequency range at each driver frequency.

The measured linear response spectra for different driver frequencies are displayed in Fig. 3. Since the ILM occurs below the linear band, the peak on the lower

frequency side of the ILM in each trace is the NF. Several peaks observed between the ILM and the linear band are linear local modes (LLMs). Here we only focus on the LLM closest to the ILM and we call it the 1st LLM.

The amplitude curve of the AR-ILM is shown in Fig. 4(a). The difference frequencies of the NF and 1st LLM with respect to the driver are presented in Fig. 4(b). When approaching the lower end of the stable region, the NF frequency difference decreases. Similar to that found for the saddle-node bifurcation in the Duffing oscillator [24], the lower transition point occurs when the NF frequency difference goes close to zero.

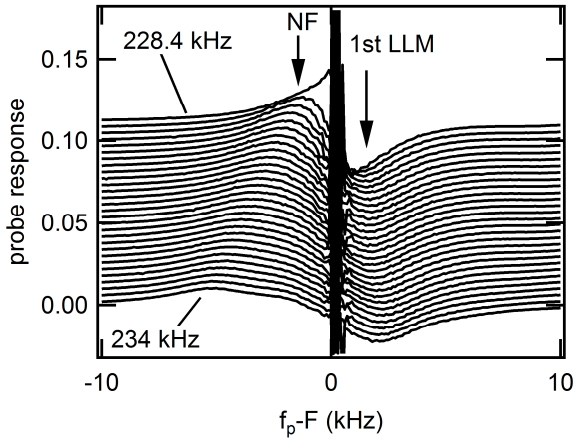

Fig. 3: Experimental imaginary part of the linear response as a function of the difference frequency between probe f_p and driver F. The frequency region of the driver ranges from 234 kHz to 228.4 kHz with 0.2 kHz steps. "NF" denotes natural frequency of the ILM, and "1st LLM" indicates the linear local mode (LLM) whose frequency is nearest the driver frequency.

3. Conclusions

We have demonstrated that an ILM can be successfully generated below the bottom of the linear wave spectrum with the MOS-FET combination as a new nonlinear element in a nonlinear electrical lattice. Since the MOS-FET combination gives rise to a large nonlinearity when its capacitance increases suddenly and saturates immediately as the applied absolute voltage increases, as shown in Fig. 1(a). The ILM remains stable inside the AR region maintained by a cw driver, which compensates the energy lose from damping. At the ends of the AR region the ILM disappears at two fundamental bifurcation transition points. By means of linear response measurements it has been shown that the behavior of the NF of the ILM plays a key role at the lower bifurcation transition. As shown in Fig. 3 and Fig. 4(b), the NF of the ILM approaches that of the driven ILM, as the driver frequency decreases. At the low frequency bifurcation point the frequency difference between the NF of the ILM and the driven ILM goes to zero. This bifurcation transition is a saddle-node type and has been studied in detail in MEMS experiments [24].

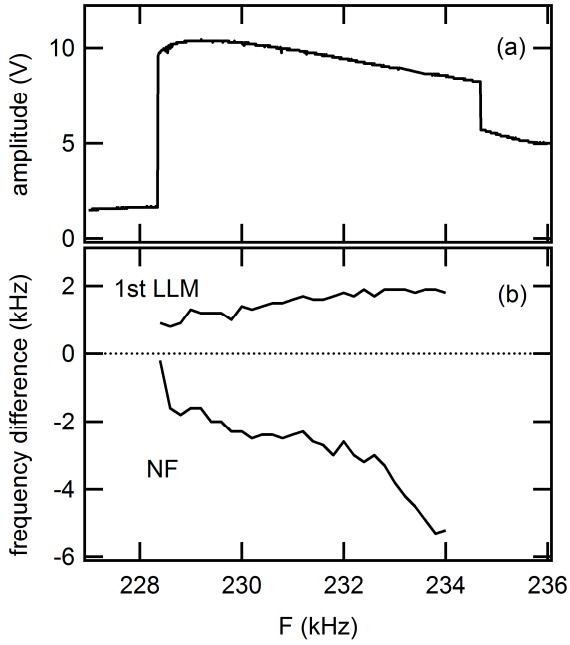

Fig. 4: (a) Amplitude of ILM as a function of the driver frequency. (b) NF and 1st LLM frequency difference versus the driver frequency. The NF difference goes to zero as the lower bifurcation point is approached.

Acknowledgements

WS was supported by the NEC C&C foundation for travel funds. MS was supported by JSPS-Grant-in-Aid for Scientific Research No. 25400391. AJS was supported by Grant NSF-DMR-0906491.

References

[1] S. Flach and A. V. Gorbach, Phys. Rep. **467**, 1 (2008).
[2] E. Trías, J. J. Mazo, and T. P. Orland, Phys. Rev. Lett. **84**, 741 (2000).
[3] P. Binder, D. Abraimov, A. V. Ustinov, S. Flach, and Y. Zolotaryuk, Phys. Rev. Lett. **84**, 745 (2000).
[4] M. Sato and A. J. Sievers, Nature **432**, 486 (2004).
[5] H. S. Eisenberg, Y. Silberberg, R. Morandotti, A. R. Boyd, and J. S. Aitchison, Phys. Rev. Lett. **81**, 3383 (1998).
[6] M. Sato, B. E. Hubbard, A. J. Sievers, B. Ilic, and H. G. Craighead, Europhys. Lett. **66**, 318 (2004).
[7] M. E. Manley, M. Yethiraj, H. Sinn, H. M. Volz, A. Alatas, J. C. Lashley, W. L. Hults, G. H. Lander, and J. L. Smith, Phys. Rev. Lett. **96**, 125501 (2006).

[8] M. E. Manley, A. Alatas, F. Trouw, B. M. Leu, J. W. Lynn, Y. Chen, and W. L. Hults, Phys. Rev. B **77**, 214305 (2008).
[9] M. E. Manley, A. J. Sievers, J. W. Lynn, S. A. Kiselev, N. I. Agladze, Y. Chen, A. Llobet, and A. Alatas, Phys. Rev. B **79**, 134304 (2009).
[10] M. Sato, B. E. Hubbard, L. Q. English, A. J. Sievers, B. Ilic, D. A. Czaplewski, and H. G. Craighead, Chaos **13**, 702 (2003).
[11] M. Sato, S. Imai, N. Fujita, S. Nishimura, Y. Takao, Y. Sada, B. E. Hubbard, B. Ilic, and A. J. Sievers, Phys. Rev. Lett. **107**, 234101 (2011).
[12] J. Fajans and L. Frièdland, Am. J. Phys. **69**, 1096 (2001).
[13] Y. Gopher, L. Friedland, and A. G. Shagalov, Phys. Rev. E **72**, 036604 (2005).
[14] A. Barak, Y. Lamhot, L. Friedland, and M. Segev, Phys. Rev. Lett. **103**, 123901 (2009).
[15] T. Kuusela, Chaos, Solitons & Fractals **5**, 2419 (1995).
[16] B. Z. Essimbi and D. Jäger, J. Phys. D **39**, 390 (2006).
[17] J. T. Pan, W. Z. Chen, F. Tao, and W. Xu, Phys. Rev. E **83**, 016601 (2011).
[18] R. Stearrett and L. Q. English, J. Phys. D **40**, 5394 (2007).
[19] L. Q. English, F. Palmero, A. J. Sievers, P. G. Kevrekidis, and D. H. Barnak, Phys. Rev. E **81**, 046605 (2010).
[20] L. Q. English, F. Palmero, P. Candiani, J. Cuevas, R. Carretero-González, P. G. Kevrekidis, and A. J. Sievers Phys. Rev. Lett. **108**, 084101 (2012).
[21] R. Van Buskirk and C. Jeffries, Phys. Rev. A **31**, 3332 (1985).
[22] M. Sato, S. Yasui, M. Kimura, T. Hikihara, and A. J. Sievers, Europhys. Lett. **80**, 30002 (2007).
[23] D. K. Schroder, *Semiconductor material and device characterization*, 2nd ed. (John Wiley & Sons, New York, 1998), Chapt. 6.
[24] M. Sato, S. Imai, N. Fujita. W. Shi, Y. Takao, Y. Sada, B. E. Hubbard, B. Ilic, and A. J. Sievers, Phys. Rev. E **87**, 012920 (2013).